European Heart Journal – Cardiovascular Imaging (2015) **16**, 1232–1240
doi:10.1093/ehjci/jev072

Temporal and spatial characteristics of the area at risk investigated using computed tomography and T_1-weighted magnetic resonance imaging

Jesper van der Pals, Sophia Hammer-Hansen, Sonia Nielles-Vallespin, Peter Kellman, Joni Taylor, Shawn Kozlov, Li-Yueh Hsu, Marcus Y. Chen, and Andrew E. Arai*

National Heart, Lung and Blood Institute (NHLBI), National Institutes of Health (NIH), Building 10, Room B1D416, MSC 1061, 10 Center Drive, Bethesda, MD 20892-1061, USA

Received 7 December 2014; accepted after revision 5 March 2015; online publish-ahead-of-print 16 April 2015

Aims Cardiovascular magnetic resonance (CMR) imaging can measure the myocardial area at risk (AAR), but the technique has received criticism for inadequate validation. CMR commonly depicts an AAR that is wider than the infarct, which in turn would require a lateral perfusion gradient within the AAR. We investigated the presence of a lateral perfusion gradient within the AAR and validated CMR measures of AAR against three independent reference standards of high quality.

Methods and results Computed tomography (CT) perfusion imaging, microsphere blood flow analysis, T_1-weighted 3T CMR and fluorescent microparticle pathology were used to investigate the AAR in a canine model ($n = 10$) of ischaemia and reperfusion. AAR size by CMR correlated well with CT ($R^2 = 0.80$), microsphere blood flow ($R^2 = 0.80$), and pathology ($R^2 = 0.74$) with good limits of agreement [$-0.79 \pm 4.02\%$ of the left ventricular mass (LVM) vs. CT; $-1.49 \pm 4.04\%$ LVM vs. blood flow and $-1.01 \pm 4.18\%$ LVM vs. pathology]. The lateral portion of the AAR had higher perfusion than the core of the AAR by CT perfusion imaging (40.7 ± 11.8 vs. 25.2 ± 17.7 Hounsfield units, $P = 0.0008$) and microsphere blood flow (0.11 ± 0.04 vs. 0.05 ± 0.02 mL/g/min, lateral vs. core, $P = 0.001$). The transmural extent of MI was lower in the lateral portion of the AAR than the core (28.2 ± 10.2 vs. $17.4 \pm 8.4\%$ of the wall, $P = 0.001$).

Conclusion T_1-weighted CMR accurately quantifies size of the AAR with excellent agreement compared with three independent reference standards. A lateral perfusion gradient results in lower transmural extent of infarction at the edges of the AAR compared with the core.

Keywords area at risk • myocardial perfusion • MRI • CT • myocardial infarction • myocardial ischaemia

Introduction

The area at risk (AAR) represents the amount of myocardium that is hypoperfused during a coronary occlusion. Over time, myocardial necrosis develops in a wavefront manner starting in the endocardial layer and extending towards the epicardium of the AAR.[1] Salvage can be calculated as the difference between the infarct size and the AAR, and represents a measure of treatment efficacy.

Changes in myocardial water content occurring early during acute myocardial infarction (MI) allow quantification of the AAR by cardiovascular magnetic resonance (CMR) imaging.[2,3] Although the extent of oedematous tissue declines over time, CMR imaging 1 week after an MI has shown excellent agreement with myocardial perfusion SPECT, the most validated clinical measure of AAR.[4] In spite of this, doubt has been raised on the feasibility of using T_2-weighted images to correctly measure the AAR based on technical concerns, physiological issues, and a lack of a true pathological reference standard.[5] From a technical standpoint, effects of surface coil proximity along with motion-related signal loss and static cavity blood may lead to artifacts that mimic myocardial oedema. Physiologically, limited oedema in reversibly injured myocardium compared with infarcted myocardium may cause problems related to the ratio of

* Corresponding author. Tel: +1 301 496 3658; Fax: +1 301 402 2389, E-mail: araia@nih.gov

contrast to noise between AAR and normal myocardium.[6,7] Also, many validation studies depict an AAR that is wider than the endocardial surface length of the infarct, a factor listed as potentially contradictory to the wavefront of myocardial necrosis in acute MI.[1,5,8] The functional relevance of the coronary collateral circulation and the possible presence of a lateral perfusion gradient within the AAR has been a matter of prolonged debate, at least partially because of inadequate means for collateral measurement.[9]

Since many of the studies on the pathophysiology of infarct development predate modern high spatial resolution *in vivo* imaging techniques, the aim of the present study was to investigate the presence of a lateral perfusion gradient, using multiple time points of computed tomography (CT) perfusion imaging and myocardial blood flow analysis. The aim was also to assess the ability of CMR to accurately detect the AAR, using a 3-T scanner and the T_1-weighted Modified Look-Locker Inversion-Recovery (MOLLI) sequence. Independent reference standards for AAR included 320-detector row CT perfusion imaging, myocardial blood flow measurements by microspheres, and pathological methods.

Methods

An overview of the experimental time line and set-up is presented in *Figure 1*.

Animal preparation

In total, 10 mongrel dogs of either sex weighing 25–30 kg were studied in accordance with the protocols approved by the Animal Care and Use Committee of the National Institutes of Health (protocol number H-0104). Anaesthesia was induced by subcutaneous acepromazine (0.2 mg/kg) followed by intravenous thiopental sodium (15 mg/kg), and sustained with inhaled sevoflurane (0.5–2.0%) after intubation. Surgical preparation included venous catheters, arterial lines, a left atrial catheter, and a snare around the left anterior descending (LAD) coronary artery positioned distal to the first diagonal branch. Coronary occlusion was maintained for 2 h followed by 90 min of reperfusion prior to CMR imaging. At the end of the experiment, the animals were euthanized using potassium chloride.

Multislice CT

Multislice CT studies were performed immediately on occlusion of the LAD using a 320 detector row scanner (Aquilion ONE Vision Edition, Toshiba Medical Systems, Otawara, Japan). The animals were supine, and the scans were acquired in volume mode during a breath hold. A standardized imaging protocol was applied using the following parameters: 0.5 mm slice thickness, 275 ms tube rotation time, 80 kV tube voltage, 750 mA tube current. Arterial phase first pass imaging was performed with continuous acquisition over 30 s with ECG gating during intravenous administration of iodinated contrast (Isovue 370, Bracco Diagnostics, Princeton, NJ, USA) 2 mL/kg divided into two injections to minimize beam hardening effects: contrast 0.8 mL/kg followed by 0.8 mL/kg

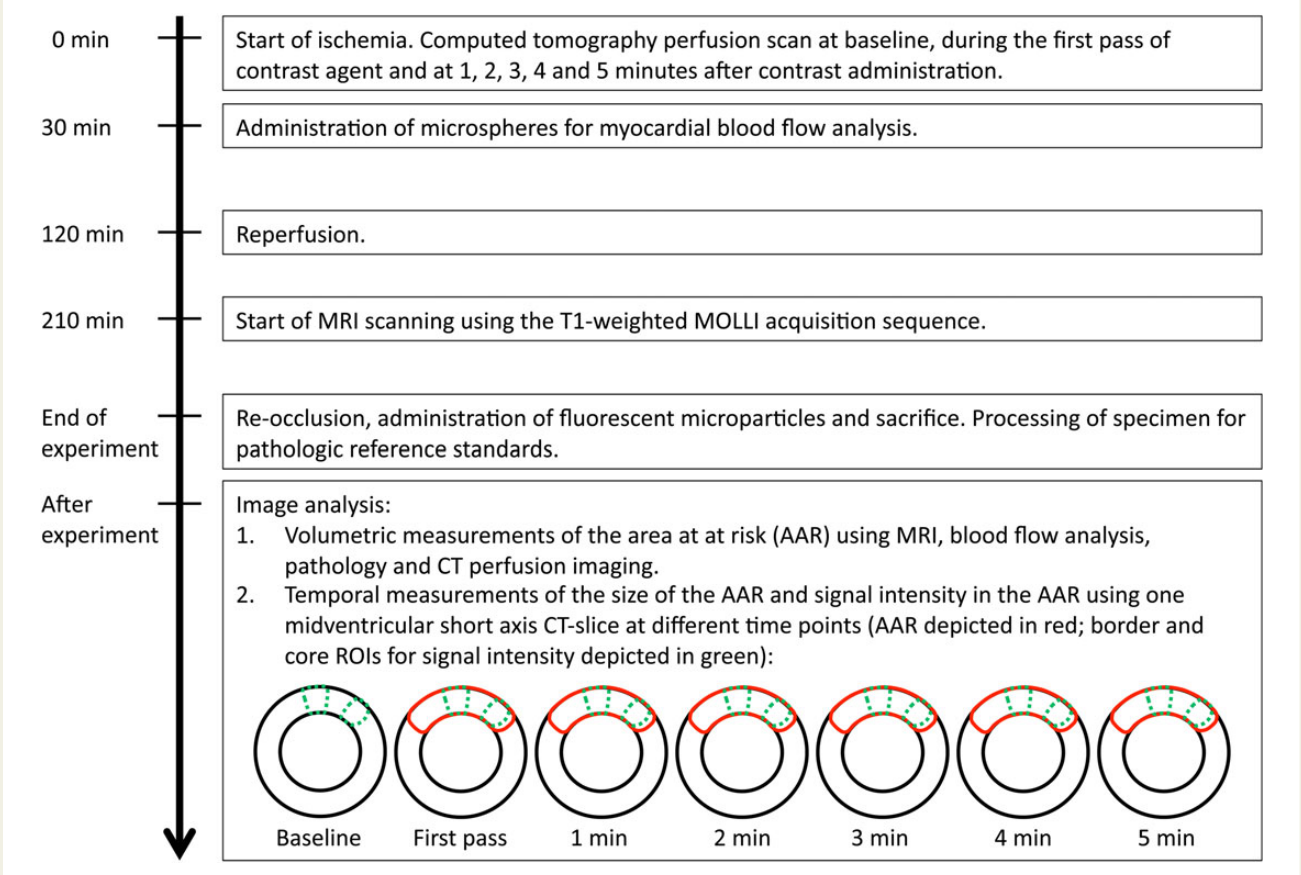

Figure 1 Experimental timeline.

saline bolus at a rate of 0.8 mL/s was immediately followed by contrast 1.2 and 1.2 mL/kg saline at a rate of 1.2 mL/s. Continuous imaging with ECG gating over five heartbeats was then acquired every minute starting at 60 s after initiation of contrast administration until minute five. Images were reconstructed at 0.5 mm slice thickness using standard cardiac kernels (FC03) with iterative reconstruction (AIDR3D) at multiple cardiac phases. Images with the least amount of motion artifact were selected for analysis.

Cardiac magnetic resonance

The CMR studies were started after a period of 90 min of reperfusion, during which time the animals were stabilized. The exams were conducted on a 3-T scanner (Magnetom Skyra, Siemens Healthcare Sector, Erlangen, Germany) in a supine position, with electrocardiographic triggering, dedicated cardiac surface coils, and expiratory breath holds. Determination of the cardiac axes with localizers was followed cine CMR acquired, using a balanced steady-state-free precession sequence. Then, T_1 was quantified with a Modified Look-Locker Inversion-Recovery (MOLLI) sequence with consecutive slices, encompassing the whole left ventricle without any gaps between the slices.[10] Typical parameters were as follows: bandwidth 1085 Hz, echo spacing/echo time 2.7/1.12 ms; flip angle 20°; field of view read 270 mm; field of view phase 75%; matrix 192 × 120 pixels; slice thickness 8 mm; parallel imaging factor 2; acquisition in late diastole; minimum inversion time 90 ms; increment 80 ms and voxel size 1.4 × 1.7 × 8.0 mm but reconstructed at a resolution of 0.7 × 0.7 × 8.0 mm. The image acquisition scheme used two inversions with images acquired for 5 s after the first inversion pulse, followed by a 3-s pause, in turn followed by a second inversion pulse and image acquisition for 3 s. The protocol is referred to as 5 s(3 s)3 s.[11]

Microsphere blood flow analysis and pathology

Microspheres for blood flow analysis (NuFlow Hydro-Coat Flow Cytometer Microspheres FM5, $n = 2.5 \times 10^6$; IMT Laboratories, Irvine, CA, USA) were injected into the left atrium at 30 min of ischaemia during simultaneous withdrawal of a reference femoral artery blood sample. Fluorescent microparticles for analysis of the AAR (Fluoro-Max

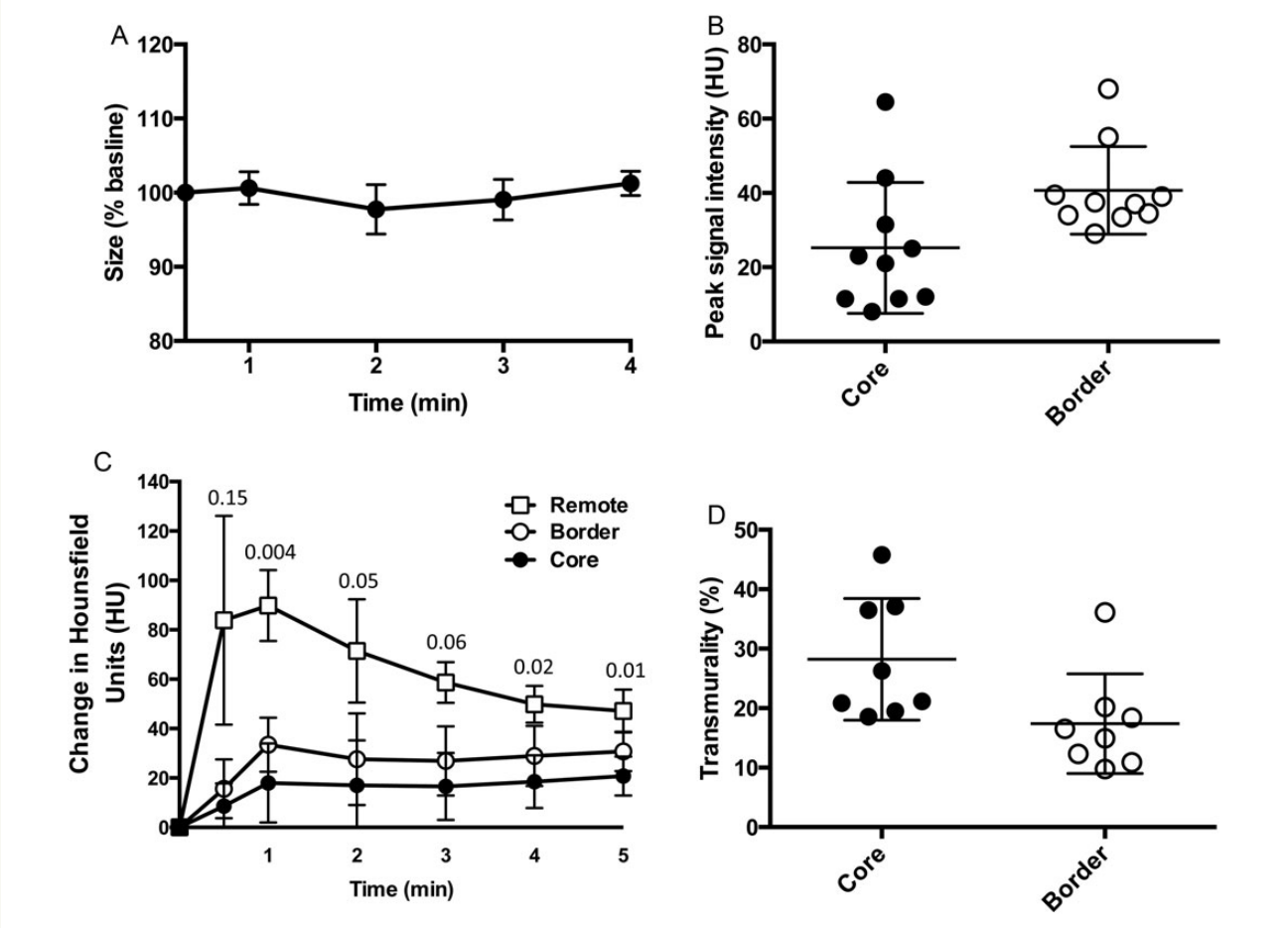

Figure 2 Temporal characteristics of the AAR. (*A*) Size of the AAR over time as measured by CT perfusion using one mid-ventricular slice at different time points. At 3 min, the size of the AAR was 99.0 ± 2.7% of the size at the earliest measured time point, $n = 7$, P = NS. (*B*) The lateral portion of the AAR was perfused to a higher degree than the core of the AAR when measured by CT perfusion imaging (peak density: 40.7 ± 11.8 vs. 25.2 ± 17.7 HU, border vs. core, $P = 0.0008$). (*C*) The change in Hounsfield Units over time in all three ROI. The peak CT contrast uptake was observed during the first pass, or ≤2 min after injection in all animals. The *P*-values for the individual time points from a comparison between the border and the core are displayed in the graph. (*D*) The higher lateral blood flow translated into a lower transmural extent of the infarct at the border than in the core of the infarct.

Fluorescent Polymer Microspheres 34-1, 500 mg suspended in 20 mL of 0.9% saline with 0.01% Tween 20; Thermo Scientific, Freemont, CA, USA) were administered at re-occlusion prior to sacrifice. Upon explantation, the hearts were set in 2% agarose gel and thereafter sliced in ~4 mm thick slices. Each slice was stained with triphenyl tetrazolium chloride (TTC) and photographed under ultraviolet and white light for demarcation of the infarcted myocardial region and the AAR. Thereafter, the slices were subsectioned into 16 transmural radial sections and sent for quantification of microsphere blood flow.

Image analysis

Volumeteric analysis of the entire perfusion defect and the left ventricle was based on reconstructed short-axis CT slices from the first pass of contrast agent, with a voxel size of 0.5 × 0.5 × 4 mm. Temporal analysis of the perfusion defect was based on one mid-ventricular short-axis slice with a voxel size of 0.5 × 0.5 × 0.5 mm at baseline, during the first pass of contrast agent and thereafter once every minute until minute 5. At these time points, the size of the AAR was analysed along with the signal intensity, as measured by Hounsfield units, in the core of the perfusion defect and in the lateral margin of the perfusion defect. The peak and change in Hounsfield units were used as semi-quantitative indices of perfusion. The change in Hounsfield units from pre- to post-contrast is directly proportional to iodine concentration and correlates with perfusion during the first pass of contrast. The regions of interest (ROI) used for signal intensity analysis were ~5 mm wide, transmural, and were placed in the central part of the perfusion defect and 2 mm from the lateral border. Microsphere data were also analysed for blood flow within the AAR, where myocardial sectors in the core of the AAR were compared with sectors located between the core and border to avoid partial volume error. Microsphere data were matched with CT analysis of perfusion, using a Vitrea® workstation with software that allows for three-dimensional reconstruction and therefore a close match between analysed segments.

All CT and MRI analyses were performed semi-automatically, using custom software where the endocardium and epicardium were manually delineated. The AAR was then automatically determined on T_1 maps, using a threshold of 2 SD higher than mean remote myocardial T_1. On CT images, the AAR was defined as 2 SD lower than mean remote myocardial Hounsfield units. The threshold values were only used in the image and subject from which it was derived. Spurious, non-contiguous voxels were manually corrected.

Evaluation of the pathological reference standard based on TTC for infarct size and fluorescent microparticles for the AAR was performed manually using the same software. Microsphere blood flow data were also analysed for size measurement of the AAR, where myocardial sectors with blood flow 2 SD below the mean blood flow in the remote myocardium were defined as the AAR.

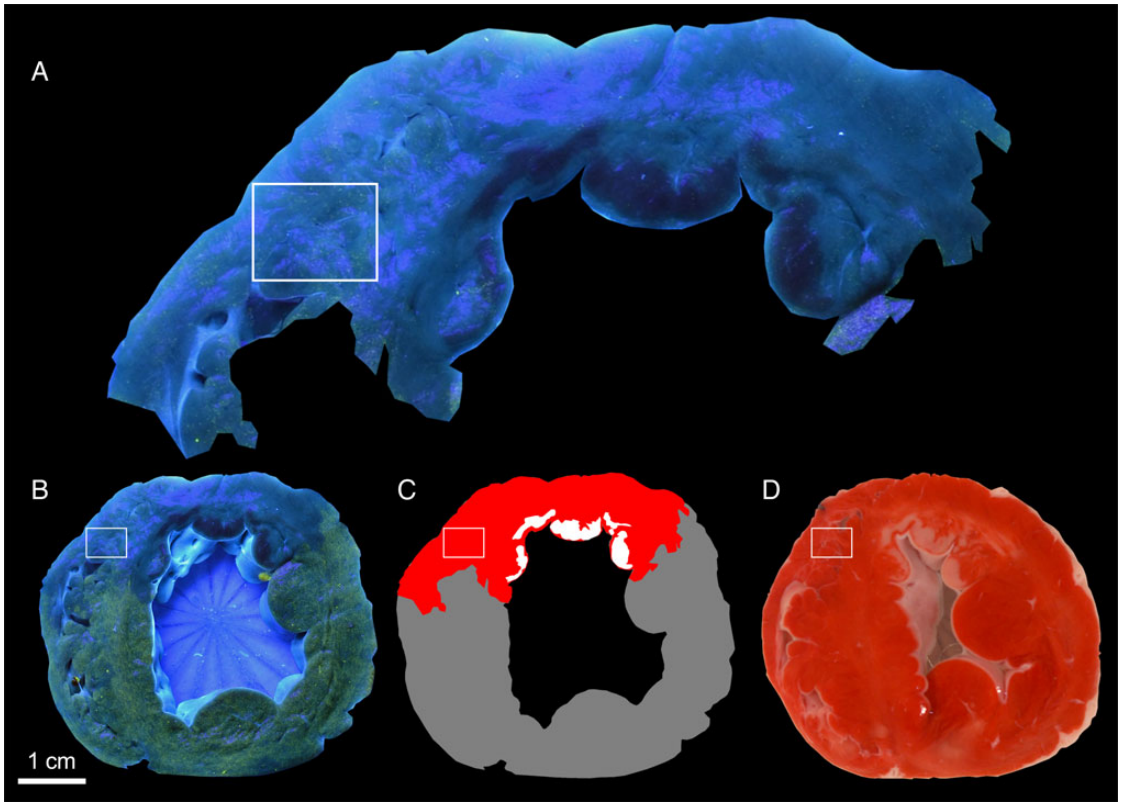

Figure 3 AAR determined by fluorescent microparticles and infarct size determined by TTC. (*A*) The AAR region extracted from the pathological sample shows some fluorescent microparticles in the AAR in the rectangle as well as in other areas. (*B*) At lower resolution, the AAR looks nearly devoid of fluorescent microparticles while remote myocardium has substantial yellow-green fluorescence. Note also the interdigitations of AAR and remote myocardium do not extend into the rectangular region of interest. (*C*) Schematic diagram of AAR (red), infarcted myocardium (white), and remote myocardium (gray). (*D*) Infarcted myocardium appears as pale patches on the cut surface of the TTC-stained myocardium.

Statistical analysis

Data analysis was performed with GraphPad Prism (Version 6.0; GraphPad Software Inc., La Jolla, CA, USA), using linear regression, Bland–Altman, or Student's *t*-test as appropriate. Results are presented as mean ± SD unless otherwise specified. Two-sided *P*-values <0.05 were considered statistically significant.

Results

Cine-MRI showed anteroapical akinesia or dyskinesia with a distinct hinge region in all animals. The blood flow in the core of the AAR during ongoing ischaemia was reduced to 7.6 ± 5.0% of the blood flow in the remote myocardium. The resultant infarct was found to be smaller than the AAR and sub-endocardial in distribution in all animals (infarct size: 6.5 ± 4.2% LVM; AAR: 32.1 ± 6.4% LVM as measured by pathology analysis). All experimental animals survived the experiment and contribute with data to all analyses apart from one unsuccessful *ex vivo* staining.

Temporal characteristics of the AAR

Based on serial CT perfusion images during the first 4 min of coronary occlusion, the size of the AAR did not change over the course of the first 4 min of ischaemia, *Figure 2*.

However, the lateral portion of the AAR was found to be perfused to a higher degree than the core of the AAR when measured by CT perfusion imaging (peak signal intensity: 40.7 ± 11.8 vs. 25.2 ± 17.7 HU, border vs. core, $P = 0.0008$). A higher CT peak signal intensity is consistent with higher x-ray contrast concentration and thus higher perfusion. Similarly, blood flow by microsphere analysis was higher in the lateral portion than in the core of the AAR (0.11 ± 0.04 vs. 0.05 ± 0.02 mL/g/min, intermediate vs. core, $P = 0.001$).

The higher blood flow in the lateral edges of the AAR translated into a lower transmural extent of the infarct near the lateral border compared with the core of the infarct (17.4 ± 8.4 vs. 28.2 ± 10.2% of the left ventricular wall, border vs. core, $P = 0.001$, *Figure 2*), measured at a level corresponding to the level where the blood flow measurements were made. Expressed in mm, this corresponds to 1.7 ± 1.0 vs. 3.7 ± 0.8 mm, border vs. core, $P = 0.0001$. The mean difference in transmural extent of infarction was 1.9 ± 0.7 mm. Two animals were excluded from this analysis due to unsuccessful staining and no discernible infarct, respectively.

The mean distance between the border of the infarct and the border of the AAR was 2.6 ± 1.2 mm (range 1.3–5.3 mm). Examples of the images used to determine pathological size of the AAR with fluorescent microparticles and infarct size with TTC are shown in *Figure 3*.

Spatial characteristics of the AAR and validation of MRI against three reference standards

The AAR was found to encompass approximately one-third of the left ventricle and was similar when measured by all modalities, *Figure 4*. *Figure 5* illustrates a representative example from all imaging modalities.

With respect to validation of the size of the AAR determinations, the correlations between MRI vs. CT, blood flow, and pathology were excellent as measured by linear regression. Bland–Altman analysis showed minimal systemic bias, generally within ~1.5% of the total LV mass, *Figure 6*.

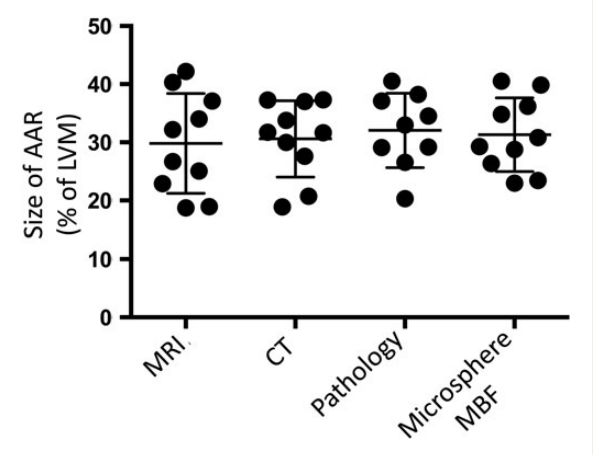

Figure 4 Spatial characteristics of the AAR. The mean AAR was similar for all imaging modalities (MRI: 30 ± 9 vs. CT: 31 ± 7 vs. Pathology: 32 ± 6 vs. Microsphere blood flow: 31 ± 6% LVM, P = NS). The threshold for demarcation of the AAR was a difference of two standard deviations from the signal intensity or blood flow in remote myocardium for MRI, CT, and microsphere blood flow analysis. Pathology analysis was performed manually. The solid line denotes mean ± SD.

The MRI MOLLI images were acquired at 216 ± 75 min after reperfusion. The T_1 relaxation time was longer in the AAR than in the remote myocardium (1462 ± 70 vs. 1245 ± 69 ms, AAR vs. remote, $P < 0.0001$; mean of differences 217 ± 48 ms). The physiological parameters recorded during the experiment are presented in *Table 1*.'

Discussion

This study examined the temporal and spatial characteristics of the AAR, using CT perfusion imaging, CMR, microsphere blood flow, and pathology analysis. The size of the AAR was found to be stable over time by CT perfusion. There was good agreement between measurements of AAR performed during the occlusion (CT and microspheres) as well as post-reperfusion methods (T_1 maps by MOLLI MRI), and by pathology. Controversial issues related to the degree of perfusion at the edges of the AAR were addressed by CT perfusion and by microspheres. Both methods showed clear evidence that blood flow was higher in the lateral part of the perfusion defect than in the core. Furthermore, there were pathophysiological consequences of the perfusion gradient at the edges of the AAR. The transmurality of infarction at the edge of the AAR as measured by TTC was less severe than that in the core of the AAR, a pattern inversely related to the measures of perfusion in these two subregions of the AAR. In addition, the infarcted myocardium did not extend to the edges of the AAR on average by 2.6 mm but in individual infarctions as much as 5.3 mm. The AAR as measured by post-reperfusion T_1 maps generated from MOLLI MRI correlated well with the other imaging modalities and pathology. The results have

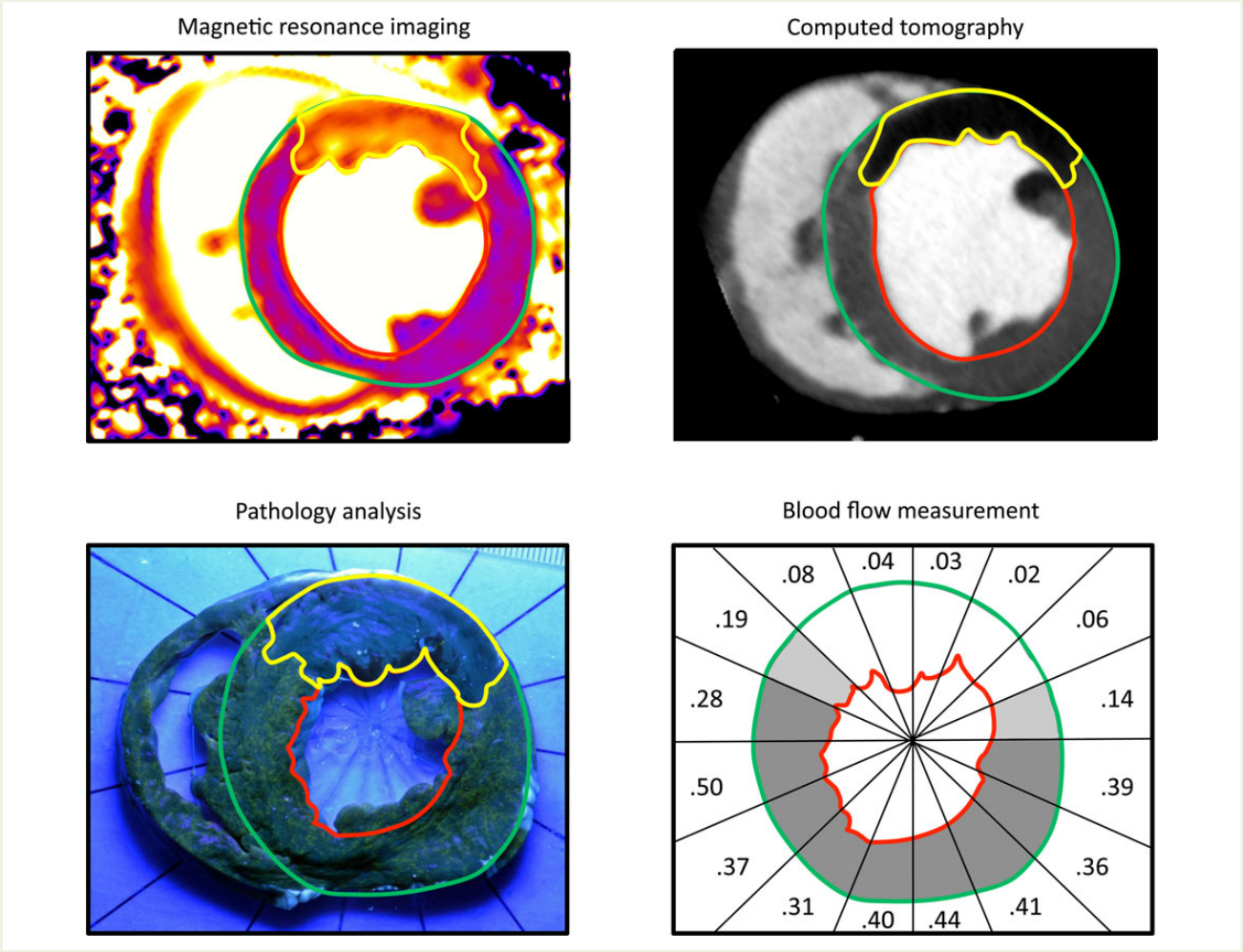

Figure 5 Representative examples of AAR imaging modalities. The AAR is delineated in yellow, endocardium in green, and epicardium in red. On MRI images, the AAR was determined using a threshold of two standard deviations (SD) higher than mean remote myocardial T_1. On CT images and blood flow measurements, the AAR was determined using a threshold 2 SD below mean remote myocardial Hounsfield units and mean remote myocardial blood flow, respectively. Digitized pathology images were segmented manually. The MRI images were acquired using the MOLLI T_1-mapping protocol. Perfused myocardium turns green-yellow under black light during pathology analysis. A thin rim of infarct (dark) is also visible. The numbers in the blood flow map represent blood flow in mL/min/g.

several important implications with respect to the pathophysiology of MI and for imaging methods used to assess myocardial salvage.

First, consistent with the presence of a lateral perfusion gradient, the lateral portion of the AAR was perfused to a higher degree than the core of the perfusion defect. We thereby provide a pathophysiological explanation for an AAR being wider than the endocardial surface length of the infarct, a common but previously unexplained feature of many validation studies of AAR delineation by CMR.[5] The properties and interdependence of the coronary perfusion beds in the context of ischaemia have been investigated previously.[9] While there has been consensus that coronary arteries are functional end-arteries in the sense that an occlusion leads to infarction, there has been contradictory results and a prolonged debate regarding the effects of vascular connections between adjacent coronary arteries on residual blood flow. Some have found that the coronary beds are interconnected by a rich network of collateral vessels,[12,13] and that the capillary level loses a tree like configuration and instead forms a three-dimensional matrix,[14] in line with the existence of a lateral perfusion gradient. Others have found coronary arteries to be end-arteries without overlap or vascular connections on the capillary level, producing discrete perfusion territories.[15,16] Collateral vessels have been suggested to produce similar flow in the medial compared with the lateral AAR,[17,18] but also to generate a higher flow near the lateral border.[19–21] Adjacent vascular territories have also been found to interdigitate with peninsulas of myocardium perfused by different coronary arteries in a manner that could cause sampling error and a false perception of a lateral perfusion gradient.[22]

Many of the prior studies have used low spatial resolution techniques (such as silicone rubber injection compounds) or methods that do not allow for serial measurements over time (such as dyes) in the same animal. However, the present study used high-resolution CT perfusion imaging with repeated measurements over time with

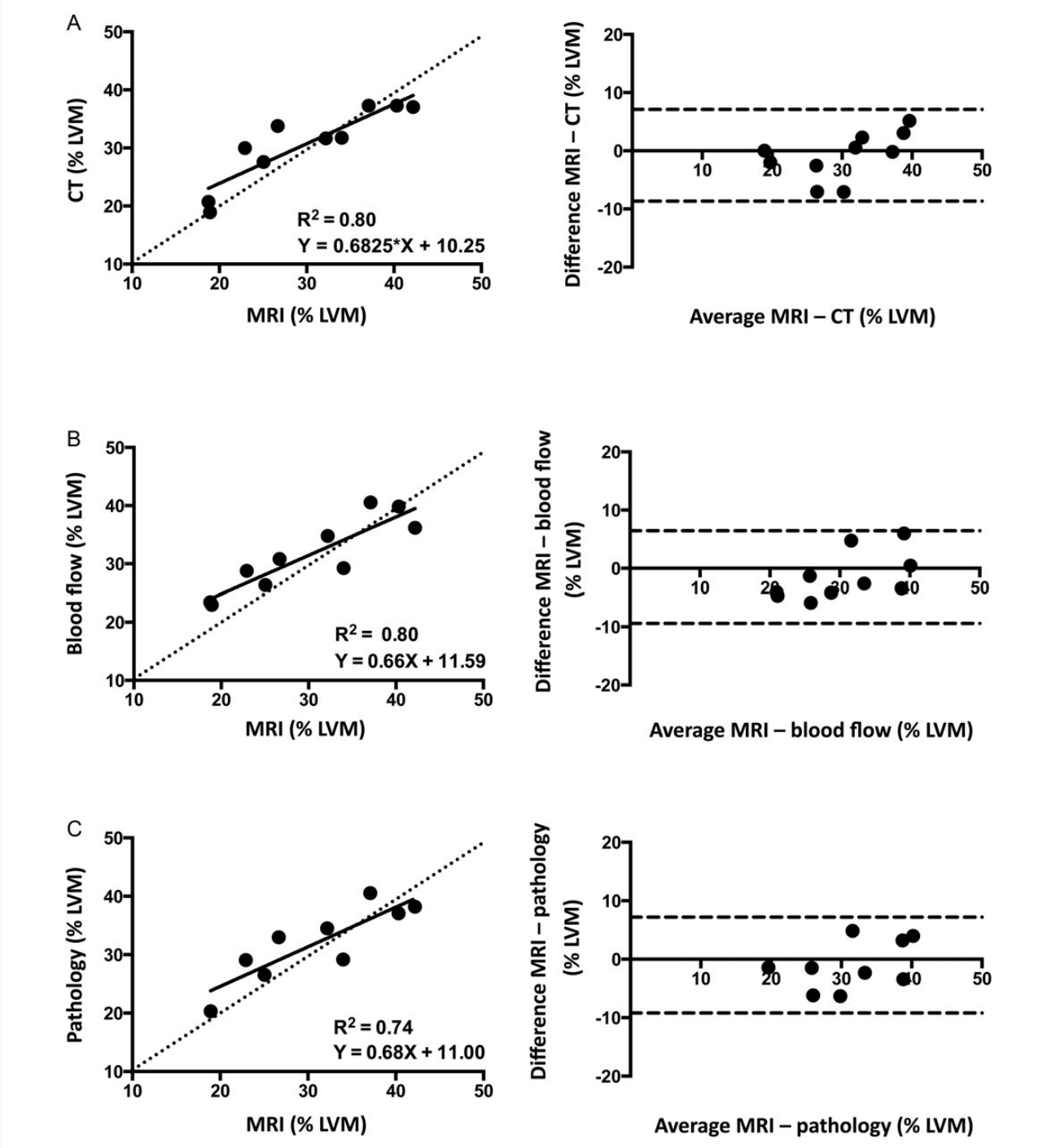

Figure 6 Agreement between MRI vs. CT, blood flow, and pathology. AAR by MRI using the MOLLI acquisition sequence is compared with AAR by (*A*) CT, (*B*) blood flow measurements, and (*C*) pathology analysis. The mean differences between the imaging methods were −0.79 ± 4.02% LVM for CT, −1.49 ± 4.04% LVM for blood flow, and −1.01 ± 4.18% LVM for pathology. The dashed lines denote the line of identity in the scatterplots and the mean ± 2 SD in the Bland–Altman plots.

identical ROI, conceivably compensating for both of these issues. Myocardial microsphere-based blood flow data gave a similar impression in the current experiment but the size of the sectors analysed precluded investigation of subtle issues at the edges of the AAR based on this modality. The stable size of the perfusion defect over time could explain the distinct drop in perfusion between remote myocardium and the AAR observed in prior studies,[18] while still allowing for a perfusion gradient within the AAR.

Secondly, the increased perfusion near the lateral border translated into a gap between the border of the perfusion defect and

Table 1 Physiological parameters during the experiment

Animal	Baseline		During ischaemia		Reperfusion (during image acquisition)	
	HR (bpm)	BP (mmHg)	HR (bpm)	BP (mmHg)	HR (bpm)	BP (mmHg)
1	88	n/a	96	96/58	83	97/48
2	108	n/a	94	70/45	95	80/50
3	89	n/a	100	80/53	102	87/55
4	121	n/a	70	95/62	62	93/59
5	114	n/a	114	75/59	113	70/52
6	124	n/a	121	78/53	123	99/56
7	77	n/a	72	95/59	80	73/54
8	89	n/a	96	76/50	95	80/51
9	95	n/a	75	94/57	88	85/56
10	77	n/a	63	85/56	76	100/66
Average	98		90	84/55	91	86/55
SD	17		19	10/5	18	11/5

The physiological parameters recorded during the experiment are presented above. Blood pressure monitoring was not available at baseline.

the border of the infarct, as previously described.[1,8] Also, the most lateral aspect of the infarct was found to have a reduced transmural extent of infarction compared with the core of the infarct at a mid-ventricular level corresponding to where the blood flow measurements were made using CT. While further supporting the presence of a lateral perfusion gradient, it should be noted that infarct development is known to be uneven and often produces myocardial scarring with complex distribution patterns.[23] Also, infarct development is not solely dependent on blood flow and oxygen/nutrient availability but also on energy expenditure.[24] This phenomenon contributes to the well-known wavefront of infarct development starting in the endocardial layer and extending towards the epicardium,[1,8] and may also explain why experimental models of MI often produce infarcts disproportionally located towards the apical portion of the AAR.

Thirdly, the AAR as measured by post-reperfusion CMR using the T_1-weighted MOLLI acquisition sequence was found to agree well with the size of the perfusion defect as measured by CT. It also agreed well with measures of the AAR based on myocardial blood flow and pathology analysis based on the distribution of fluorescent microparticles. Previous experimental studies have shown that T_1 values increase in parallel with increasing myocardial water content.[25,26] Prolonged T_1 values have also been observed in ischaemic myocardium in humans and animals.[27,28] Specifically, the MOLLI acquisition protocol has been compared against myocardial blood flow and T_2-weighted CMR for measurement of the AAR, using a 1.5 T scanner in experimental MI.[29] The present experiment confirms the finding of a close agreement between the modalities and adds a validation against CT perfusion imaging and *ex vivo* pathology analysis. It also moves the concept of T_1-weighted CMR using MOLLI for AAR analysis onto a 3 T platform. While it should be noted that the coronary circulation of the dog — in contrast to the healthy human — is characterized by a high number of naturally occurring collaterals (and therefore does not make the translation to human AMI completely straightforward), the MOLLI acquisition sequence appears overall well suited for analysis of the AAR in the context of clinical trials on candidate cardioprotective drugs. Indeed, a shortened version of the protocol known as ShMOLLI has been demonstrated to detect myocardial oedema in patients with acute MI at least as well as T_2-weighted CMR and also to correlate with functional improvement at 6 months.[30]

Fourthly, the MOLLI T_1-mapping protocol used in the current experiment may reduce the artifacts inherent to some of the more widely used T_2-weighted protocols for detection of the AAR.[5,6] The MOLLI protocol is a bright blood acquisition sequence. Therefore, it does not suffer from some problems that affect the more conventional black-blood T_2-weighted protocols, where static cavity (bright) blood adjacent to hypokinetic (bright) myocardium and motion-related myocardial signal loss in the remote myocardium may cause artifacts that mimic the AAR. In a similar way, T_2 parametric mapping might quantify AAR more accurately than T_2-weighted imaging.

Limitations

The present study was performed using state-of-the-art, high spatial, and temporal resolution techniques in order to address the questions put up for investigation. Nevertheless, it has some limitations that merit consideration. One aspect is that all modalities have inherent strengths and limitations that are different from each other. In order to facilitate direct comparison between these, normalization to left ventricular mass was used in order to reduce effects of shrinkage during *ex vivo* processing and possible effects of image acquisition at slightly different phases of the cardiac cycle. The need of co-registration and fusion of images was reduced by using pathology instead of non-invasive imaging for analysis of the spatial distribution and relationship between scar and AAR. Furthermore, since the analysis of myocardial blood flow was performed during the first minutes of ischaemia, later changes in the pathophysiology dependent on necrosis and microvascular obstruction are beyond the reach of the analysis of the lateral perfusion gradient. However, the observed effects on the

infarct (with a gap between infarct and perfused myocardium, and an edge of the AAR with reduced transmural extent of infarction) indicate that the pathophysiology is consistent throughout ischaemia and reperfusion. Due to the fact that the analysis of blood flow was based on mid-ventricular myocardium, it is not possible to draw firm conclusions regarding the blood flow on more apical and basal levels. Also, the present experiment does not address the question whether the AAR in itself is affected by treatment with a cardioprotective agent.[31] Nevertheless, we believe that the findings in the present study to be of significant value for the scientific community in providing a stable method for imaging of the AAR and a basis for further refinement of the technique.

Conclusions

In conclusion, a lateral perfusion gradient exists within the mid-ventricular perfusion territory of the LAD during myocardial ischaemia in the canine. The T_1-weighted MOLLI sequence sensitively and accurately quantifies the AAR with excellent agreement compared with CT perfusion imaging, myocardial blood flow measurements, and histopathology.

Acknowledgements

The authors thank Katherine Lucas and Stephanie French for expert animal care and laboratory assistance.

Conflict of interest: A.E.A. has a cooperative research and development agreement with Siemens Medical. A.E.A. and M.Y.C. also have research agreements with Toshiba Medical.

Funding

This work was funded by the Division of Intramural Research, National Heart, Lung and Blood Institute, National Institutes of Health (grant numbers ZIA HL004607-15, ZIC HL005909-06, ZIA HL006136-03, ZIA HL006138-03 and ZIA HL006136-04). The contents and views of this paper are solely the responsibility of the authors and do not necessarily represent the official views of the National Institutes of Health. Funding to pay the Open Access publication charges for this article was provided by the National Heart, Lung and Blood Institute (NHLBI), National Institutes of Health (NIH), Bethesda, Maryland, USA.

References

1. Reimer KA, Jennings RB. The "wavefront phenomenon" of myocardial ischemic cell death. II. Transmural progression of necrosis within the framework of ischemic bed size (myocardium at risk) and collateral flow. *Lab Invest* 1979;**40**:633–44.
2. Garcia-Dorado D, Oliveras J, Gili J, Sanz E, Perez-Villa F, Barrabes J *et al.* Analysis of myocardial oedema by magnetic resonance imaging early after coronary artery occlusion with or without reperfusion. *Cardiovasc Res* 1993;**27**:1462–9.
3. Aletras AH, Tilak GS, Natanzon A, Hsu LY, Gonzalez FM, Hoyt RF Jr *et al.* Retrospective determination of the area at risk for reperfused acute myocardial infarction with T2-weighted cardiac magnetic resonance imaging: histopathological and displacement encoding with stimulated echoes (DENSE) functional validations. *Circulation* 2006;**113**:1865–70.
4. Carlsson M, Ubachs JF, Hedstrom E, Heiberg E, Jovinge S, Arheden H. Myocardium at risk after acute infarction in humans on cardiac magnetic resonance: quantitative assessment during follow-up and validation with single-photon emission computed tomography. *JACC Cardiovasc Im* 2009;**2**:569–76.
5. Croisille P, Kim HW, Kim RJ. Controversies in cardiovascular MR imaging: T2-weighted imaging should not be used to delineate the area at risk in ischemic myocardial injury. *Radiology* 2012;**265**:12–22.
6. Friedrich MG, Kim HW, Kim RJ. T2-weighted imaging to assess post-infarct myocardium at risk. *JACC Cardiovasc Im* 2011;**4**:1014–21.
7. Wince WB, Kim RJ. Molecular imaging: T2-weighted CMR of the area at risk--a risky business? *Nature Rev* 2010;**7**:547–9.
8. Reimer KA, Lowe JE, Rasmussen MM, Jennings RB. The wavefront phenomenon of ischemic cell death. 1. Myocardial infarct size vs duration of coronary occlusion in dogs. *Circulation* 1977;**56**:786–94.
9. Zimarino M, D'Andreamatteo M, Waksman R, Epstein SE, De Caterina R. The dynamics of the coronary collateral circulation. *Nature Rev* 2014;**11**:191–7.
10. Messroghli DR, Greiser A, Frohlich M, Dietz R, Schulz-Menger J. Optimization and validation of a fully-integrated pulse sequence for modified look-locker inversion-recovery (MOLLI) T1 mapping of the heart. *J Magn Res Im* 2007;**26**:1081–6.
11. Kellman P, Hansen MS. T1-mapping in the heart: accuracy and precision. *J Cardiovasc Magn Res Im* 2014;**16**:2.
12. Helfant RH, Vokonas PS, Gorlin R. Functional importance of the human coronary collateral circulation. *NEJM* 1971;**284**:1277–81.
13. Fulton FW, VanRoyean N. The coronary collateral circulation in man. In: Schaper W, Schaper J, ed. *Arteriogenesis*. Dordrecht, the Netherlands: Kluwer Academic Publishers; 2004. p297–331.
14. Kassab GS, Fung YC. Topology and dimensions of pig coronary capillary network. *Am J Physiol* 1994;**267**:319–25.
15. Factor SM, Okun EM, Minase T, Kirk ES. The microcirculation of the human heart: end-capillary loops with discrete perfusion fields. *Circulation* 1982;**66**:1241–8.
16. Okun EM, Factor SM, Kirk ES. End-capillary loops in the heart: an explanation for discrete myocardial infarctions without border zones. *Science* 1979;**206**:565–7.
17. Reimer KA, Long JB, Murry CE, Jennings RB. Three-dimensional distribution of collateral blood flow within the anatomic area at risk after circumflex coronary artery occlusion in dogs. *Bas Res Cardiol* 1987;**82**:473–85.
18. Yellon DM, Hearse DJ, Crome R, Wyse RK. Temporal and spatial characteristics of evolving cell injury during regional myocardial ischemia in the dog: the "border zone" controversy. *J Am Coll Cardiol* 1983;**2**:661–70.
19. Leong-Poi H, Coggins MP, Sklenar J, Jayaweera AR, Wang XQ, Kaul S. Role of collateral blood flow in the apparent disparity between the extent of abnormal wall thickening and perfusion defect size during acute myocardial infarction and demand ischemia. *J Am Coll Cardiol* 2005;**45**:565–72.
20. Sabia PJ, Powers ER, Jayaweera AR, Ragosta M, Kaul S. Functional significance of collateral blood flow in patients with recent acute myocardial infarction. A study using myocardial contrast echocardiography. *Circulation* 1992;**85**:2080–9.
21. Kaul S, Pandian NG, Guerrero JL, Gillam LD, Okada RD, Weyman AE. Effects of selectively altering collateral driving pressure on regional perfusion and function in occluded coronary bed in the dog. *Circ Res* 1987;**61**:77–85.
22. Axford-Gatley RA, Wilson GJ. The "border zone" in myocardial infarction. An ultrastructural study in the dog using an electron-dense blood flow marker. *Am J Pathol* 1988;**131**:452–64.
23. Moon JC, De Arenaza DP, Elkington AG, Taneja AK, John AS, Wang D *et al.* The pathologic basis of Q-wave and non-Q-wave myocardial infarction: a cardiovascular magnetic resonance study. *J Am Coll Cardiol* 2004;**44**:554–60.
24. Dunn RB, Griggs DM Jr. Transmural gradients in ventricular tissue metabolites produced by stopping coronary blood flow in the dog. *Circ Res* 1975;**37**:438–45.
25. Brown JJ, Peck WW, Gerber KH, Higgins CB, Strich G, Slutsky RA. Nuclear magnetic resonance analysis of acute and chronic myocardial infarction in dogs: alterations in spin-lattice relaxation times. *Am Heart J* 1984;**108**:1292–7.
26. Higgins CB, Herfkens R, Lipton MJ, Sievers R, Sheldon P, Kaufman L *et al.* Nuclear magnetic resonance imaging of acute myocardial infarction in dogs: alterations in magnetic relaxation times. *Am J Cardiol* 1983;**52**:184–8.
27. Williams ES, Kaplan JI, Thatcher F, Zimmerman G, Knoebel SB. Prolongation of proton spin lattice relaxation times in regionally ischemic tissue from dog hearts. *J Nucl Med* 1980;**21**:449–53.
28. Goldfarb JW, Arnold S, Han J. Recent myocardial infarction: assessment with unenhanced T1-weighted MR imaging. *Radiology* 2007;**245**:245–50.
29. Ugander M, Bagi PS, Oki AJ, Chen B, Hsu LY, Aletras AH *et al.* Myocardial edema as detected by pre-contrast T1 and T2 CMR delineates area at risk associated with acute myocardial infarction. *JACC Cardiovasc Im* 2012;**5**:596–603.
30. Dall'Armellina E, Piechnik SK, Ferreira VM, Si QL, Robson MD, Francis JM *et al.* Cardiovascular magnetic resonance by non contrast T1-mapping allows assessment of severity of injury in acute myocardial infarction. *J Cardiovasc Magn Res* 2012;**14**:15.
31. Hausenloy DJ, Yellon DM. Clinical translation of cardioprotective strategies: report and recommendations of the Hatter Institute 5th International Workshop on Cardioprotection. *Basic Res Cardiol* 2008;**103**:493–500.